Electronic Supplementary Material (ESI) for Nanoscale.

Supporting Information: Binding of Polar and Hydrophobic Molecules at the $LiCoO_2$ (001)-water Interface: Force Field Development and Molecular Dynamics Simulations

Dongyue Liang,[†] Juan Liu,[‡,¶] Hendrik Heinz,[‡] Sara E. Mason,[§] Robert J. Hamers,[‖] and Qiang Cui[*,⊥]

†*Department of Chemistry and Theoretical Chemistry Institute, University of Wisconsin-Madison, 1101 University Avenue, Madison, WI 53706*

‡*Department of Chemical and Biological Engineering, University of Colorado-Boulder, Boulder, CO 80303-0596*

¶*Department of Materials Science and Engineering, Dalian Maritime University, Dalian, Liaoning 116026, China*

§*Department of Chemistry, University of Iowa, E331 Chemistry Building, Iowa City, Iowa 52242*

‖*Department of Chemistry, University of Wisconsin-Madison, 1101 University Avenue, Madison, WI 53706*

⊥*Departments of Chemistry, Physics and Biomedical Engineering, Boston University, 590 Commonwealth Avenue Boston, MA 02215*

E-mail: qiangcui@bu.edu,Tel:(+1)-617-353-6189

Table S1: Different partial charges of atoms in the LCO force field.

Type	Bader[a]	No H-ter[b]	Initial Guess[c]	Optimized[d]
Li	0.893	0.62	0.641	0.641
Co	1.341	0.98	0.962	0.962
O	-1.112	-0.8	-0.798	-0.798
OH	-1.163	-	-0.833	-0.848
OT	-0.891	-	-0.639	-0.624
HT	0.691	-	0.496	0.492

a. Charges obtained from Bader charge analysis[1–3] by averaging over atoms of the same type. b. Charges derived using the Interface Force Field protocol without consideration of surface termination, reported by Heinz, Liu, Jain and coworkers.[4] c. Charges obtained by dividing the Bader charges by a weighted scaling factor obtained between Bader charges and charges without consideration of surface terminations, which serve as the initial guess for subsequent optimization. The weighted scaling factor is obtained as the following: first, for each atom type, a scaling factor is calculated based on the partial charge in the original INTERFACE force field and the Bader charge; then an overall scaling factor is calculated by averaging over all atom types weighted by the frequency of their occurrence in the LCO material. d. Optimized charges based on matching force-field and DFT interaction energies between water probe and LCO.

Table S2: Counts of binding events between specific groups in NADH and the LCO surface, defined as the minimum distance being smaller than 2.7 Å.

Group 1	Group 2	Group 3	Group 4	Group 5	NICO	RIBO
AN7/85378	AO2'/105837	AO2[b]/296306	NO3'/163294	NO7/107408	NO7/22875	AO3[b]/1768498
AN6/72551	AO3'/67443	AO1[b]/271544	NO2'/158189	NN7/14505	NN7/2252	AO2[b]/1649626
AN1/56963	-	NO1[c]/262523	-	-	-	AO1[b]/1592398
-	-	NO2[c]/256310	-	-	-	-

a. The statistics are collected from 4 replicas of 500 ns MD trajectories with a saving frequency of 5 ps (maximum possible number of events = 15 molecules × 400,000 frames = 6,000,000). For each binding event, the atom forming the closest contact with the LCO surface is recorded, and this table summarizes all the atom types that contribute to more than 1% of the binding events in the format of type/counts. See Fig. 6 in the main text for atom types. b. oxygen atoms on AP. c. oxygen atoms on NP.

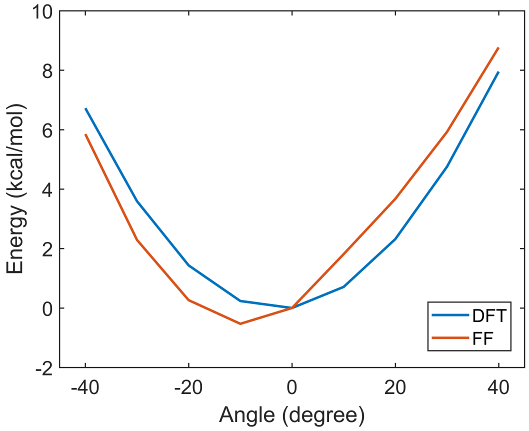

(a)

Figure S1: Comparison of energy scans for the Co-OH1(OH2)-HT angle with the plane-wave DFT and the developed force field (FF) model. The calculations are performed with the 50% hydrogen terminated LCO surface. The angle shown here is defined as the angle between the z axis and the OH1(OH2)-HT vector.

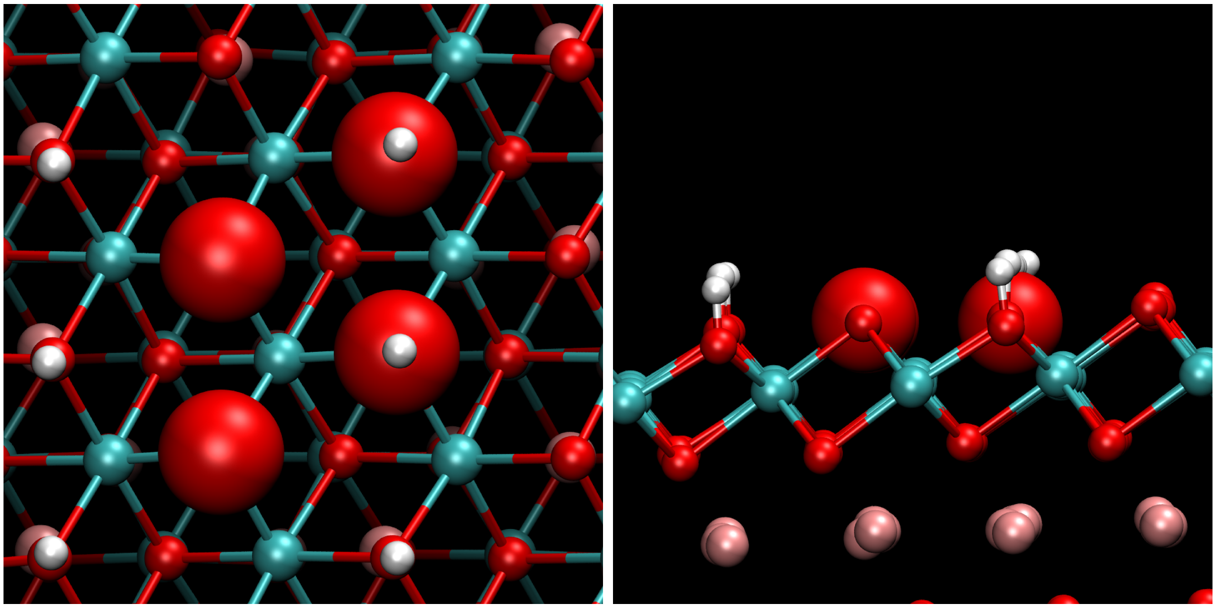

(a) (b)

Figure S2: Illustration of the surface oxygen atoms selected for defining the coordination number used in metadynamics simulations. (a) and (b) show the top and side views, respectively, with the selected oxygen atoms highlighted as larger spheres.

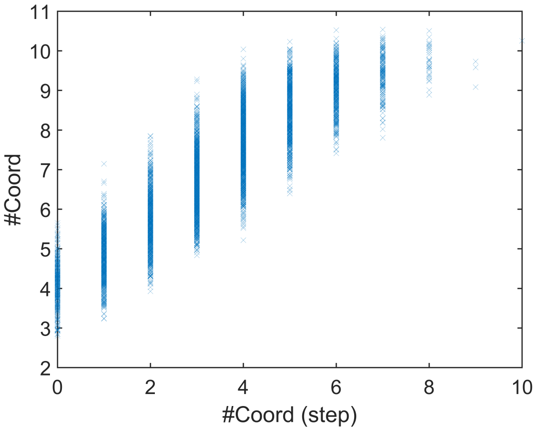

(a)

Figure S3: Scatter plot between the #Coord defined in Eq. 1 in the main text, and the coordination number where a double summation of step functions (with a threshold radius of 3.0 Å) is used instead, which is denoted as #Coord(step). The data shown here are obtained from an 80-ns metadynamics trajectory for the ACEH case. The figure indicates that the #Coord is strongly correlated with #Coord(step), but exhibits larger variations and higher average values due to the use of a smooth switching function, which includes cumulative contributions from many water molecules. As a result, variation of the free energy profile along #Coord is expected to be shallow since different coordination environments are effectively averaged over.

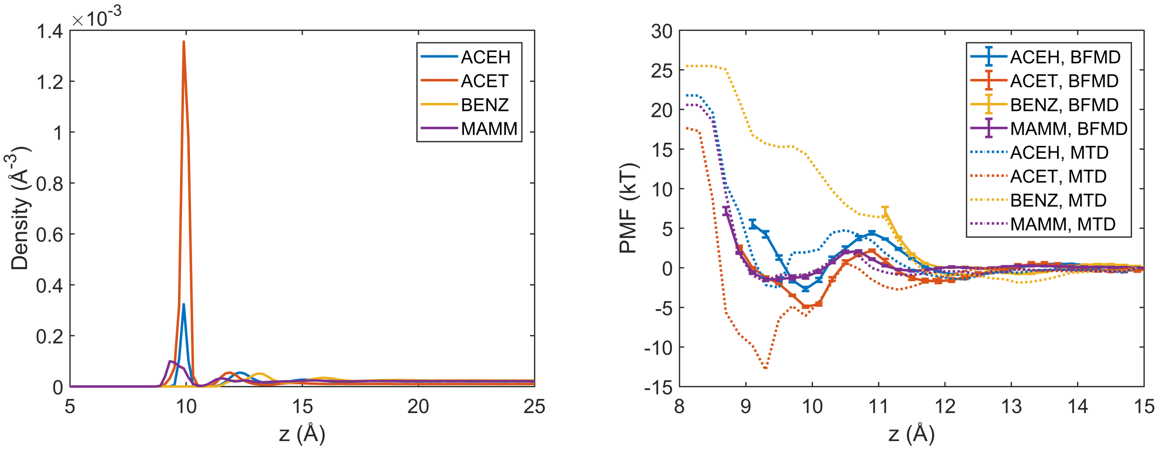

(a) (b)

Figure S4: (a) Number density profiles of small molecule adsorption on the LCO (001) surface with respect to z, which is defined as the distance between center of mass of the small molecule and center of mass of the LCO slab; for reference, the surface oxygen layer is ∼6.3 Å from the center of mass of the LCO slab. (b) Comparison between 1-dimensional PMFs calculated from the number density profiles ($W(z) = -k_BTln\rho(z)$) from unbiased, "brute-force" MD (BFMD) and integration of 2-dimensional PMF from well-tempered metadynamics (MTD). The brute force MD simulation is run for 200 ns, with 4 replicas for each system; 15 small molecules are included in each system. The well-tempered metadynamics are run for 160 ns for each small molecule.

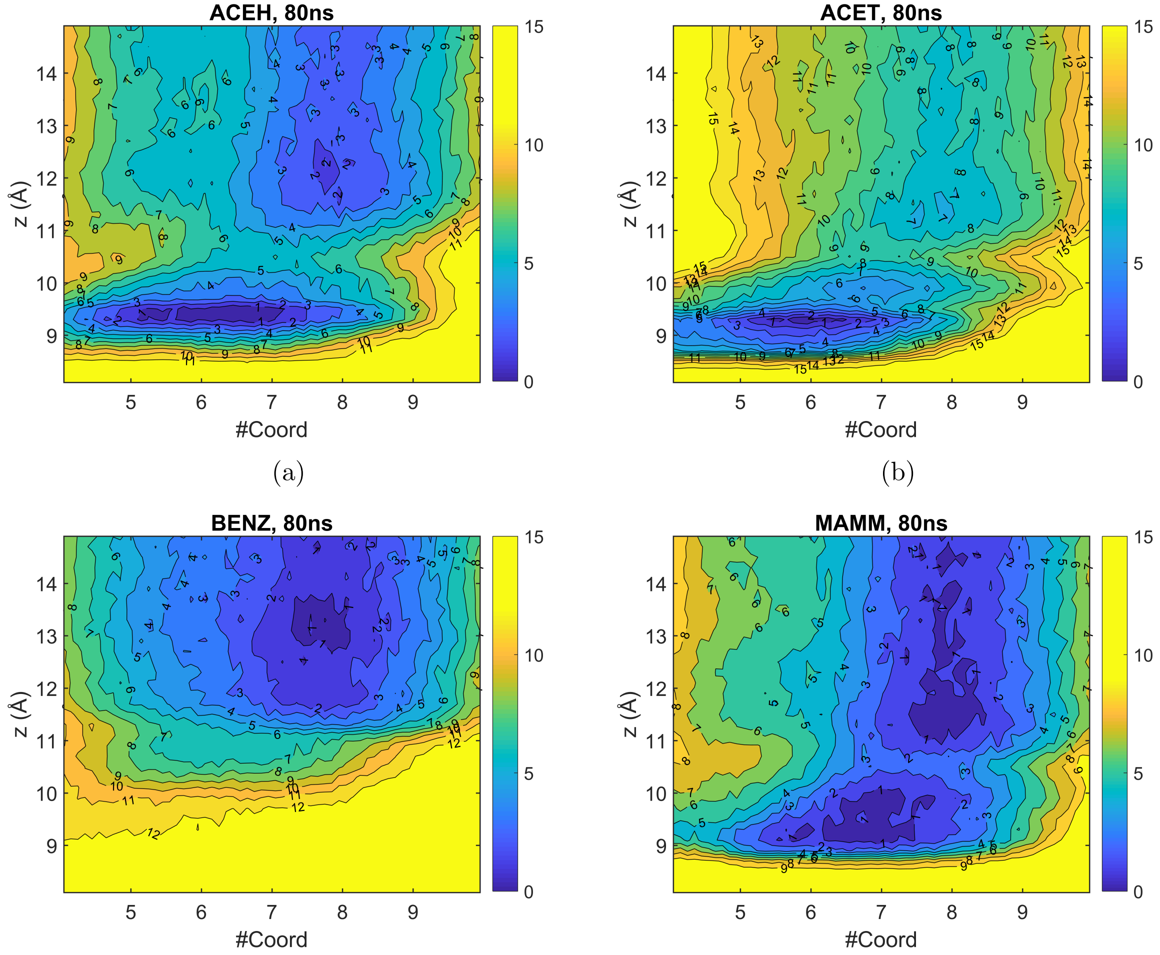

(a) (b) (c) (d)

Figure S5: Two-dimensional PMFs for the adsorption of small molecules to the LCO (001)-water interface from 80 ns well-tempered metadynamics; the results are not significantly different from the 160 ns result shown as Fig. 5 in the main text, supporting adequate convergence of the free energy surfaces.

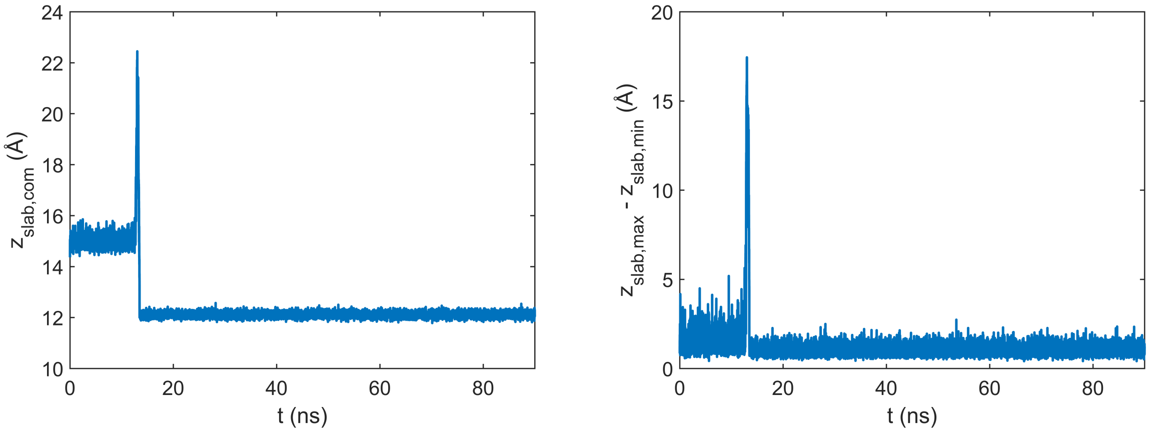

(a) (b)

Figure S6: Adsorption of a single-layer 10×10 $\mathring{A}^2$ graphene sheet to the LCO (001) surface in water during MD simulation. The figures show the time evolution of (a) the vertical center of mass separation between LCO and the graphene sheet and (b) the vertical min-max distance of the graphene slab, which characterizes the orientation of the slab at the surface. It is evident that the graphene sheet quickly settles to the location of the second layer of water with a flat orientation.

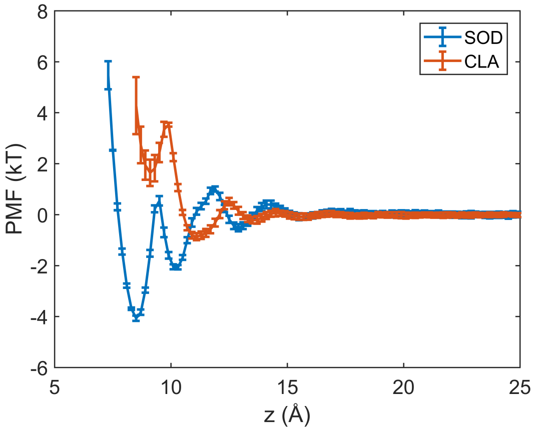

Figure S7: PMFs of sodium and chloride ions at the LCO (001)-water interface from classical MD simulations. The analysis is performed with the same unbiased MD trajectories as Fig. S4.

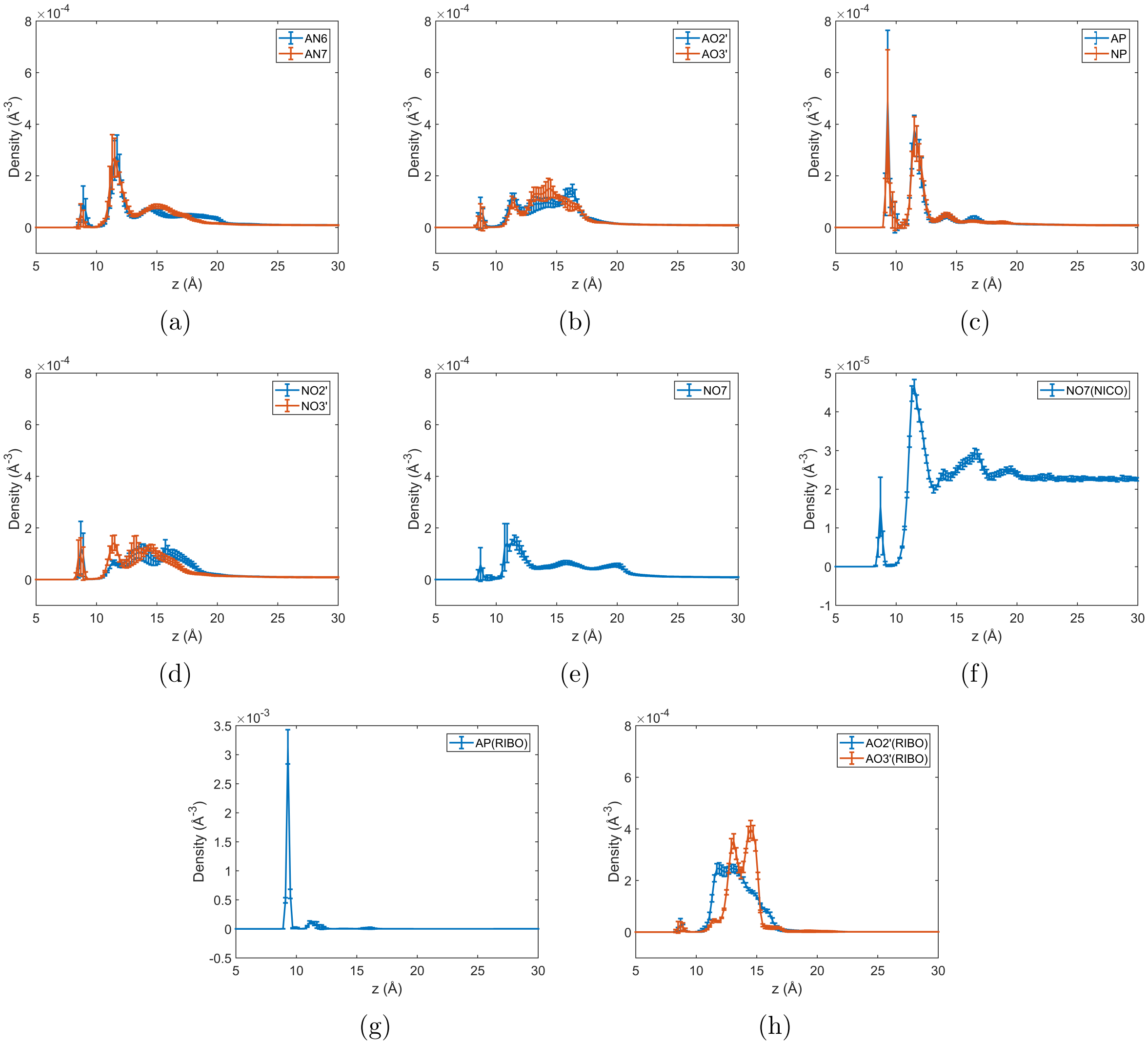

(a) (b) (c)

(d) (e) (f)

(g) (h)

Figure S8: Number density distributions for the atom of interest to the center of mass of LCO along z based on 4 replicas of 500 ns MD simulations. (a-e) show atom types from NADH, (f) from NICO, and (g-h) from RIBO. See Fig.6 of main text for the list of atom types.

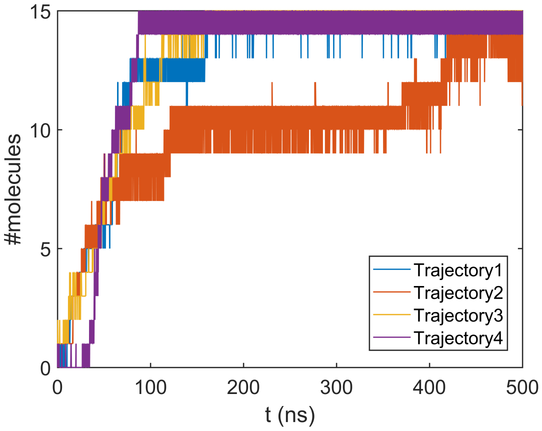

Figure S9: Time evolution of the number of RIBO molecules adsorbed on the LCO (001) surface in 4 different replicas of MD trajectories. Binding/unbinding events are not frequently sampled once the molecules are absorbed on the surface.

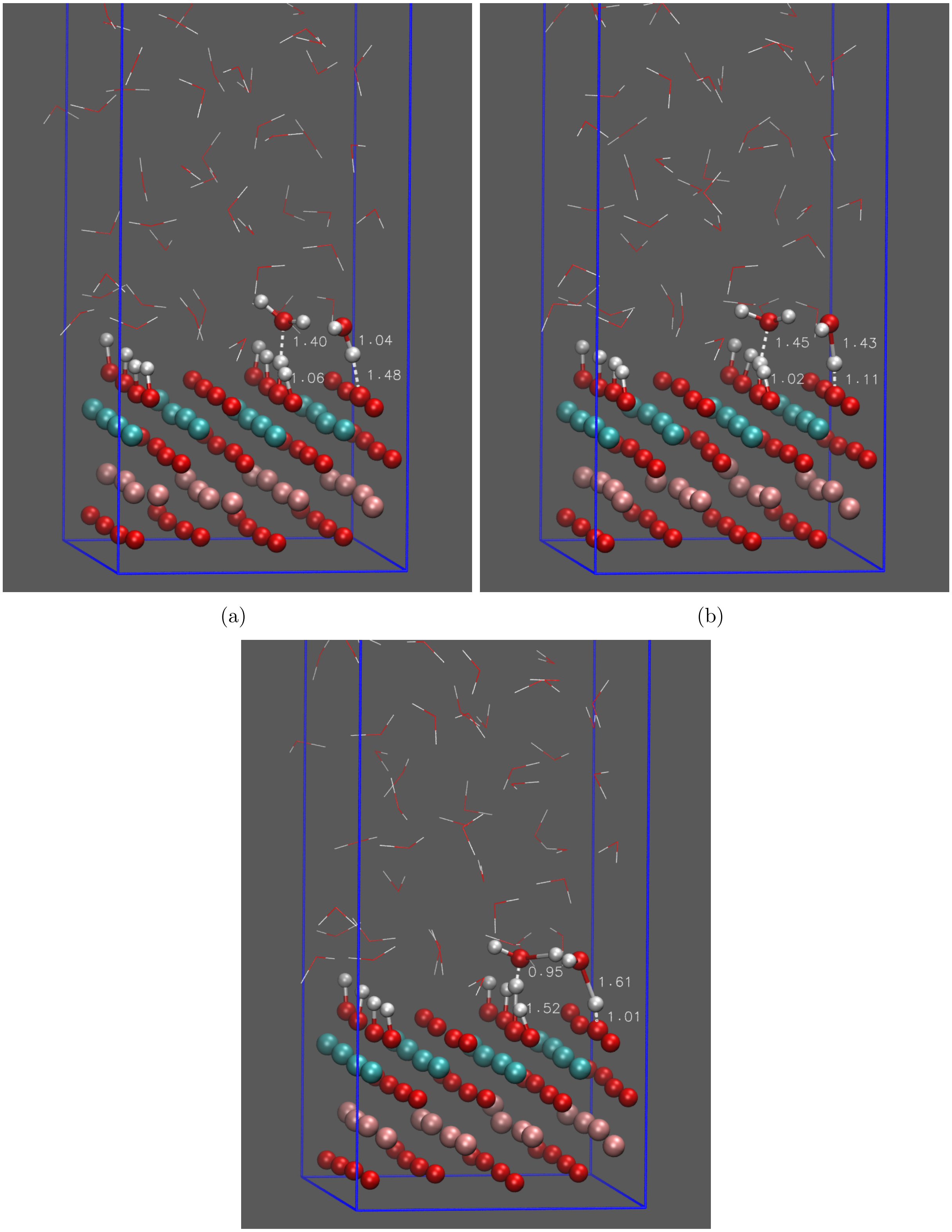

(a)

(b)

(c)

Figure S10: Snapshots that illustrate the proton transfer process at the LCO/water interface observed in the 50 ps ab initio (RPBE-D3) MD simulation.

References

(1) Tang, W.; Sanville, E.; Henkelman, G. A grid-based Bader analysis algorithm without lattice bias. *J. Phys. Condens. Matter* **2009**, *21*, 084204.

(2) Sanville, E.; Kenny, S. D.; Smith, R.; Henkelman, G. Improved grid-based algorithm for Bader charge allocation. *J. Comput. Chem.* **2007**, *28*, 899–908.

(3) Henkelman, G.; Arnaldsson, A.; Jónsson, H. A fast and robust algorithm for Bader decomposition of charge density. *Comput. Mater. Sci.* **2006**, *36*, 354–360.

(4) Dhakane, A.; Varshney, V.; Liu, J.; Heinz, H.; Jain, A. Molecular dynamics simulations of separator-cathode interfacial thermal transport in a Li-ion cell. *Surf. Interfaces* **2020**, *21*, 100674.